

Analytical Solutions for Turbulent Channel Flow Using Alexeev and Navier-Stokes Hydrodynamic Equations: Comparison with Experiments

Alex Fedoseyev

Ultra Quantum Inc., Huntsville, Alabama, USA

E-mail: af@ultraquantum.com

Abstract. Understanding turbulent boundary layer flows is important for many application areas. Enhanced theoretical models may provide deeper insights into the fundamental mechanisms of turbulence that elude current models; therefore, the search for improved kinetic equations and their respective hydrodynamic equations continues. In this work, we consider the Generalized Boltzmann Equation (GBE), proposed by Alexeev (1994). The GBE accounts for finite particle size and the variation of the distribution function over timescales of the order of the collision time. The Alexeev hydrodynamic equations are derived from the GBE. In this work, the Alexeev hydrodynamic equations (AHE) and Navier-Stokes (NS) equations are solved analytically for turbulent channel flow under the assumption that stationary solutions yield the mean flow velocity. The analytical solutions of the AHE are validated by numerical solutions and compared with the NS solutions and experimental data for turbulent channel flow from multiple sources, spanning Reynolds numbers from 3,000 to 35,000,000. Solutions of the AHE demonstrate significantly better agreement with experimental data than those obtained from the NS equations. The analytical solution revealed a new similarity parameter: the boundary layer thickness scale, which coincides with the Kolmogorov microscale observed in experiments. The mechanisms for turbulence generation and control are discussed.

Keywords: Generalized Boltzmann Equation; Alexeev Hydrodynamic Equations; Navier-Stokes equations; Turbulent channel flow; Turbulent boundary layer; Analytical solution; Numerical solution; Experimental validation.

1 Introduction

Understanding turbulent boundary layer flows is important for many application areas. Experimental investigations of turbulent channel flow provide critical data for improving theoretical and numerical models and offer insights into the fundamental mechanisms of turbulence that may not be captured by existing approaches. Enhanced theoretical models may provide deeper insights into these fundamental mechanisms; therefore, the search for improved kinetic equations, their respective hydrodynamic equations, and accurate turbulence models continues.

The proposed approach for turbulent flow solutions uses a novel theoretical model: the Alexeev hydrodynamic equations (AHE) obtained by Alexeev in 1994 [1]. The AHE were derived from the Generalized Boltzmann Equation (GBE) [1]. The GBE differs from the Boltzmann Equation (BE) by accounting for finite particle size and the variation of the distribution function over timescales of the order of the collision time. Consequently, the GBE includes a second material derivative term with a timescale coefficient.

We begin with a review of the Generalized Boltzmann Equation, its derivation and properties, and then present the Alexeev hydrodynamic equations, including the full system for incompressible flow and several simplified models. The validation of the AHE is referenced to several different authors. The derivation of the analytical solution of the AHE for turbulent channel flow is provided, and the solution is compared to the numerical solution of the AHE for validation. The results are compared to the Navier-Stokes (NS) solutions and to high-quality experimental data from multiple sources. The conclusion summarizes the results.

2 Generalized Boltzmann Equation

The standard Boltzmann transport equation accounts for changes in the distribution function $f(\mathbf{r}, \mathbf{v}, t)$ on the hydrodynamic timescale and the mean time between collisions of infinitesimal particles, which are treated as material points. Introducing a third timescale associated with the finite dimensions of interacting particles leads to an additional term in the equation: a second material derivative of the distribution function. This results in a generalized form known as the Generalized Boltzmann Equation [1]:

$$\frac{Df}{Dt} - \frac{D}{Dt} \left(\tau \frac{Df}{Dt} \right) = J^B, \quad (1)$$

where $f = f(\mathbf{r}, \mathbf{v}, t)$ is particle velocity distribution function, and operator

$$\frac{D}{Dt} = \frac{\partial}{\partial t} + \mathbf{v} \cdot \frac{\partial}{\partial \mathbf{r}} + \mathbf{F} \cdot \frac{\partial}{\partial \mathbf{v}} \quad (2)$$

represents material derivative in space, velocity space and time, and J^B is the collision integral, the same as in Boltzmann equation ([2], p.11), where \mathbf{v} and \mathbf{r} are the velocity and the position of the particle, respectively, t is the time, and \mathbf{F} is the force acting on the particle. A timescale multiplier τ is a material property.

The GBE was obtained from first principles, starting from the Liouville equation for the multi-particle distribution function f_N of a system of N interacting particles by introducing a small parameter $\varepsilon = nv_b$, where n is the number particle density, and v_b is the interaction volume. Then, starting from the hierarchy of Bogolyubov kinetic equations (chain), Alexeev broke the Bogolyubov chain at the r_b -scale, where $r_b = v_b^{1/3}$, finding the exact representation of the term [2](p.52), and obtained a one-particle representation function $f(\mathbf{r}, \mathbf{v}, t)$ resulting in the GBE equation (1). The timescale τ is introduced as:

$$\tau = \frac{\varepsilon}{[\partial \varepsilon / \partial t]_{t=0}}, \quad (3)$$

where ε is the number of particles of all kind, found themselves within the interaction volume of a particle numbered as l at the instant of time t , and the derivative $[\partial \varepsilon / \partial t]_{t=0}$ is taken at the moment $t = 0$, when the volume v_b is empty (no particles).

During the derivation of the GBE, the sign of the τ multiplier must be chosen, and the negative sign was selected to satisfy the Boltzmann H-theorem. The GBE is thermodynamically consistent and satisfies the conditions for the Boltzmann H-theorem [2].

Alexeev assumed that the parameter τ defined in this way is the mean time between collisions [2](p.52). This is not correct. It was found that the parameter τ is of much larger value, and is a material property, that, in the case of the hydrodynamic equations, gives rise to the length scale $\delta = \sqrt{\tau \nu}$, where ν is the kinematic viscosity. We will show that δ is a boundary layer thickness scale and that δ coincides with the Kolmogorov microscale observed in experiments. This δ has a value of approximately 0.6 mm for distilled water and approximately the same for air over a wide pressure range (to hundreds of atmospheres).

The spacial range of validity of the GBE extends from hydrodynamic scale L down to the mean free path between collisions λ , and further down to the particle interaction scale r_b [2]. The Alexeev hydrodynamic equations have the same range of validity as the GBE, which has been confirmed by simulations for rarefied hypersonic flows [15, 17, 16].

3 Hydrodynamic Equations

3.1 Alexeev Hydrodynamic Equations

The Alexeev Hydrodynamic Equations (AHE) were derived from the Generalized Boltzmann Equation by multiplying the latter by the standard collision invariants (mass, momentum, energy) and integrating the result over the velocity space. For incompressible flow and thermal convection, the AHE were first presented by Fedoseyev and Alexeev (1998) in [22, 23]. The main results from these papers were summarized in a book by Alexeev (2004) [2] (p. 253). The full AHE were provided in [22] and [18], and they have the following form:

$$\frac{\partial \mathbf{V}}{\partial t} + (\mathbf{V} \cdot \nabla) \mathbf{V} - \frac{1}{Re} \nabla^2 \mathbf{V} + \nabla p - \mathbf{F} = \tau \left\{ \frac{\partial^2 \mathbf{V}}{\partial t^2} + 2 \frac{\partial}{\partial t} (\nabla p) + \nabla^2 (p \mathbf{V}) + \nabla (\nabla \cdot (p \mathbf{V})) \right\} \quad (4)$$

while continuity equation is

$$\nabla \cdot \mathbf{V} = \tau \left\{ 2 \frac{\partial}{\partial t} (\nabla \cdot \mathbf{V}) + \nabla \cdot (\mathbf{V} \nabla) \mathbf{V} + \nabla^2 p - \nabla \cdot \mathbf{F} \right\} \quad (5)$$

where \mathbf{V} and p are nondimensional velocity and pressure, $Re = V_0 L_0 / \nu$ - the Reynolds number, V_0 - velocity scale, L_0 - hydrodynamic length scale, ν - kinematic viscosity, \mathbf{F} is a body force and a nondimensional τ is

$$\tau = \tau_0 L_0^{-1} V_0 = \tau_0 \nu / L_0^2 Re = \delta^2 Re, \quad (6)$$

where τ_0 is the dimensional value of τ . The parameter τ is assumed to be constant. Note that the AHE have two similarity parameters: the Reynolds number Re and the boundary layer thickness scale δ ,

$$\delta = \sqrt{\tau_0 \nu} / L_0. \quad (7)$$

Additional boundary conditions on the walls require that the fluctuations be zero: The boundary condition for pressure on the walls is

$$(\nabla p - \mathbf{F}) \cdot \mathbf{n} = 0, \quad (8)$$

where \mathbf{n} is a wall normal. These equations have been used to obtain a transient analytical solution for the transverse velocity component [13].

3.2 Simplified Alexeev Hydrodynamic Equations

A simplified model of the AHE for incompressible fluid was first presented in [20, 19]. This model has been successfully applied to a number of high Reynolds number flows and thermal convection problems, as well as to magneto-hydrodynamics [21, 4, 5, 6, 31]. We use this simplified model for stationary turbulent channel flow:

$$\frac{\partial \mathbf{V}}{\partial t} + (\mathbf{V} \cdot \nabla) \mathbf{V} - \frac{1}{Re} \nabla^2 \mathbf{V} + \nabla p = 0, \quad (9)$$

$$\nabla \cdot \mathbf{V} = \tau \nabla^2 p, \quad (10)$$

where \mathbf{V} and p are nondimensional velocity and pressure respectively, $Re = U_0 L_0 / \nu$ - the Reynolds number, U_0 - velocity scale, L_0 - hydrodynamic length scale, ν - kinematic viscosity, and nondimensional timescale $\tau = \tau_0 L_0^{-1} U_0$, where τ_0 is the dimensional timescale, a material property. The boundary condition for pressure on the walls is $(\nabla p \cdot \mathbf{n}) = 0$.

The timescale τ can be rewritten as

$$\tau = \delta^2 Re, \quad (11)$$

where

$$\delta = \frac{\sqrt{\tau_0 \nu}}{L_0}, \quad (12)$$

another similarity parameter together with the Reynolds number. Equations (9) and (10) reduce to the Navier-Stokes equations when $\tau = 0$, and their solution becomes the solution of the Navier-Stokes equations. That has been proven recently by Amosova (2023) [3].

4 Governing equations for two-dimensional channel flow and solutions

For the case of two-dimensional horizontal channel flow with width L_0 , we seek stationary solutions in half of the channel (assuming solution symmetry), under the assumption that these solutions yield the mean flow velocity. In this configuration, no variables depend on x (the streamwise direction), so all derivatives with respect to x vanish except for the pressure gradient $p_x = \text{const}$. The problem thus reduces to a one-dimensional case where all the variables depend only on y .

4.1 Stationary Navier-Stokes equations for 2D flow in channel

In the continuity equation of the Navier-Stokes equations,

$$\nabla \cdot \mathbf{V} = 0 \quad (13)$$

for velocity $\mathbf{V} = (U, V)$, the derivative $U_x = 0$, and thus

$$V_y = 0. \quad (14)$$

With the boundary condition $V(0) = 0$, this yields the solution $V = 0$ for transverse flow velocity component. The momentum equation then becomes

$$-\frac{1}{Re} U_{yy} + p_x = 0, \quad (15)$$

with the boundary condition $U(0) = 0$. Assuming the velocity at the channel centerline is $U = U_0$, the solution can be readily obtained as

$$U(y) = U_0 \cdot 4y(L - y)/L^2, \quad (16)$$

where $U_0 = \frac{1}{8} Re p_x L_0^2$. The well-known parabolic solution for the streamwise velocity was obtained, representing the laminar flow. No other solutions are possible for the stationary Navier-Stokes equations.

4.2 Stationary Alexeev hydrodynamic equations for 2D flow in channel

The AHE become the following: the momentum and continuity equations are

$$VU_y - \frac{1}{Re} U_{yy} + p_x = 0, \quad (17)$$

$$VV_y - \frac{1}{Re} V_{yy} + p_y = 0, \quad (18)$$

$$V_y = \tau p_{yy}. \quad (19)$$

with the boundary condition $V(0) = 0, U(0) = 0, U(0.5) = U_0$.

4.3 Approximate analytical solution of the Alexeev hydrodynamic equations

Finding an analytical solution to equations (17), (18), and (19) is difficult. To simplify the problem, we replace these equations with two sets of equations describing the laminar and turbulent velocity components. We assume that the general solution $U(y)$ of equations (17), (18), and (19) is a superposition of the laminar and turbulent velocity solutions, U^L and U^T ,

$$U = U_0(\gamma U^T + (1 - \gamma)U^L), \quad (20)$$

along with V

$$V = \gamma V^T, \quad (21)$$

since $V^L = 0$. The AHE equations become the following:

$$V^T(\gamma U_y^T + (1 - \gamma)U_y^L) - \frac{1}{Re}(\gamma U^T_{yy} + (1 - \gamma)U^L_{yy}) + p_x = 0, \quad (22)$$

$$V^T V_y^T - \frac{1}{Re} V^T_{yy} + p_y^T = 0, \quad (23)$$

$$V_y^T = \tau p^T_{yy}. \quad (24)$$

The first set consists of one equation: the laminar velocity component equation for U^L :

$$-\frac{1}{Re}(1 - \gamma)U^L_{yy} + p_x = 0, \quad (25)$$

with the boundary conditions $U^L(0) = 0, U^L(0.5) = U_0$, and the transverse velocity component $V^L = 0$. The solution of this equation is given by (16).

The second set consists of the turbulent velocity component equations – the momentum equations for U^T and V^T and the continuity equation – and has the form:

$$V^T(U_y^T + \alpha U_y^L) - \frac{1}{Re} U^T_{yy} = 0, \quad (26)$$

$$V^T V_y^T - \frac{1}{Re} V^T_{yy} + p_y^T = 0, \quad (27)$$

$$V_y^T = \delta^2 Re \cdot p^T_{yy}, \quad (28)$$

where τ was substituted from (11) by $\delta^2 Re$, and $\alpha = (1 - \gamma)/\gamma < 1$ is the fraction of the laminar velocity component relative to the turbulent one. The boundary conditions are $U^T(0) = 0, V^T(0) = 0, U^T(0.5) = U_0$. Equations (27) and (28) can be combined, resulting in an independent equation for V^T ,

$$\frac{1}{Re} V^T_{yy} - V^T V_y^T - \frac{1}{\delta^2 Re} V^T = 0. \quad (29)$$

We can see that the streamwise component of velocity U^T in the linear equation (26) depends on V^T , while the equation for the transverse velocity component V^T is completely independent. Equation (29) can be solved, and its solution for $V^T(y)$ can be used to solve equation (26) for $U^T(y)$.

If the second term in the equation (26) containing U_y^L is neglected, since $\alpha U_y^L \ll U_y^T$ (in the boundary layer), the solution U^T can be obtained by integrating equation (26), resulting in an analytical formula that expresses the solution $U^T(y)$ through integrals of $V^T(y)$,

$$U^T(y) = C_1 \int_1^y \exp\left(\int_1^\eta Re \cdot V^T(\xi) d\xi\right) d\eta + C_2, \quad (30)$$

where the constants C_1 and C_2 are chosen to satisfy the boundary conditions. Alternatively, equation (26) can be solved by numerical methods, e.g. the finite-difference method.

Non-trivial approximate analytical solutions of equations (26) to (28) were derived in [14], which presented the solution as an explicit formula:

$$U^T = U_0 \left(1 - e^{1-e^{y/\delta}}\right), \quad (31)$$

$$V^T = \frac{1}{\delta Re} \left(1 - e^{y/\delta}\right), \quad (32)$$

$$p_y^T = \frac{1}{\delta^2 Re} V^T. \quad (33)$$

4.4 Validation for the turbulent solution U^T

The approximate solution for V^T , equation (32), was obtained in [14] from equation (27) by dropping the nonlinear term $V^T V_y^T$, differentiating it with respect to y , and substituting the expression for p_{yy}^T into equation (28), obtaining the equation

$$V_{yyy}^T - \frac{1}{\delta^2} V_y^T = 0. \quad (34)$$

When the sign of $\delta = \sqrt{\delta^2}$ was taken as positive, the solution V^T is

$$V^T = \frac{1}{\delta Re} \left(1 - e^{y/\delta}\right). \quad (35)$$

Another solution, when the sign of $\delta = -\sqrt{\delta^2}$ was taken as negative, was considered in [11]:

$$V^T = -\frac{1}{\delta Re} \left(1 - e^{-y/\delta}\right). \quad (36)$$

The linear combination of U^T solutions, corresponding to the V^T solutions above, gave more accurate results for U^T at high Re numbers [12].

When the V^T solution (35) was substituted into the simplified equation (26) with omitted term αU_y^L , since $\alpha U_y^L \ll U_y^T$ (in the boundary layer), it was possible to solve it analytically, resulting in the solution U^T (31). Dropping the term $V^T V_y^T$ was a significant simplification but necessary step to obtain a closed-form formula. Therefore, validation of the U^T solution is required.

In the following, the numerical solution of the equations for V^T and U^T from the more accurate equations is presented:

$$\frac{1}{Re} V_{yy}^T - V^T V_y^T - \frac{1}{\delta^2 Re} V^T = 0, \quad (37)$$

$$V^T U_y^T - \frac{1}{Re} U_{yy}^T = 0. \quad (38)$$

The solution was computed for the Wei (1989) experiment at $Re = 14914$ using a finite-difference method with $N = 201$ to 401 nodes (yielding indistinguishable solutions) on a non-uniform mesh refined near the boundaries. To avoid the trivial solutions U^T and $V^T = 0$, the deflation technique proposed by Farrell (2015) was applied [9].

Equation (37) results in a nonlinear system of finite-difference equations, which was solved by minimizing the squared residual using the Powell hybrid method (MINPACK) [29]. The same approach was used to solve equation (38).

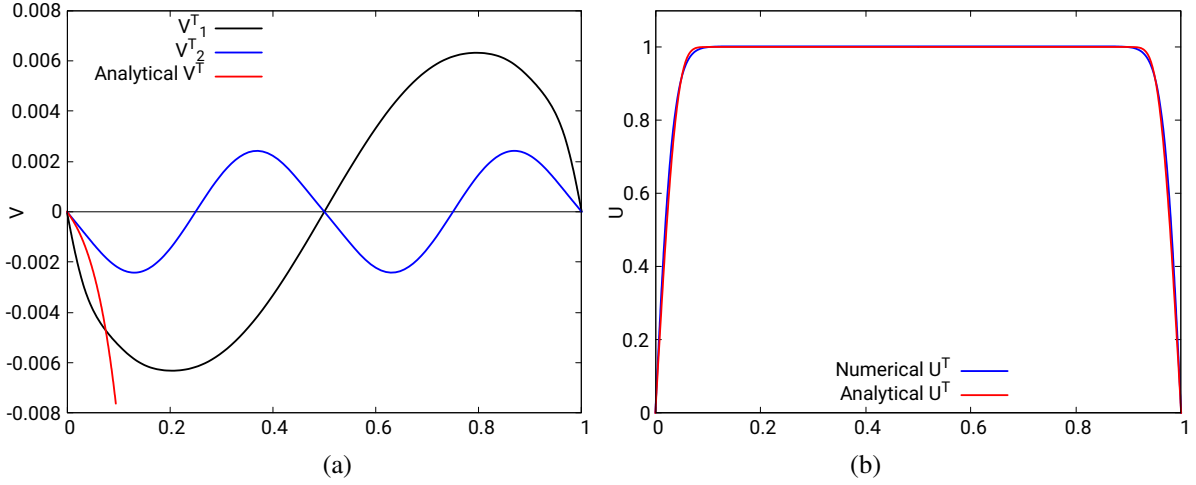


Figure 1: (a) Two numerical solutions for the transverse velocity $V^T(y)$ in the channel at $Re = 14914$, computed using equation (37). The initial approximations were $\sin(n\pi y)$, for $n = 2, 4$. The analytical solution (32) is also shown (red line). (b) The solution for the streamwise turbulent velocity $U^T(y)$ from equation (38) (blue line), corresponding to the $V_1^T(y)$ solution (the only non-zero numerical solution), and the analytical solution $U^T(y)$ (31) (red line) are shown.

It was found that equation (37) admits multiple solutions; two of them are shown in Figure 1(a). Only one of them, V_1^T , results in the non-zero $U^T(y)$ solution shown by the blue line in Figure 1(b). The analytical solution $U^T(y)$ (31) is also shown in Figure 1(b) as the red line and is very close to the numerical solution, nearly indistinguishable in the figure.

The validation provided above confirms that the approximate analytical solution U^T is in excellent agreement with the numerical solution for this Reynolds number. For very high Reynolds numbers ranging from 1,000,000 to 35,000,000, there is a larger deviation between the numerical and analytical U^T solutions; for such cases, an improved analytical solution is proposed [11].

4.5 General solution of Alexeev hydrodynamic equations

The general solution $U(y)$ for turbulent flow in channel is proposed as a linear superposition of U^L and U^T [14],

$$U(y) = U_0 \left[\gamma \left(1 - e^{1-e^{y/\delta}} \right) + (1 - \gamma) 4y(L - y)/L^2 \right], \quad (39)$$

where γ and $(1 - \gamma)$, the coefficients of superposition, that are introduced to satisfy $U(0.5) = U_0$. The analytical solution (39) can also be used for the turbulent flow in circular pipe if $\delta \ll 1$ [11]. The parameter γ is calculated through the principle of minimum viscous dissipation [12], and typically γ is close to 0.65. The dimensional value of δ , $\delta_0 = \sqrt{\tau_0 \nu}$ is approximately 0.6 mm for distilled water and air over a wide pressure range [11].

5 Comparison of analytical solutions with experiments

5.1 Comparison of solutions for channel flow: Wei and Willmarth experiments

We use experimental data for turbulent flow in a two-dimensional channel to compare solutions obtained from the Navier-Stokes equations and the Alexeev Hydrodynamic Equations. Only stationary solutions for incompressible flow are considered, under the assumption that these yield the mean flow velocity. The solutions are compared with high-quality experimental data from multiple sources.

The experiments of Wei and Willmarth (1989) [32] were done in turbulent channel flow over the range of four Reynolds number from 2970 to 39582 based on a channel half-width. The working fluid was distilled water. The analytical solutions and the experimental data for streamwise mean velocity at Reynolds number $Re = 2970$ are shown in Figure 2. The experimental velocity data are shown by circles.

Figure shows both the U^L , parabolic solution (laminar, green line), that is the Navier-Stokes solution, and U^T , super-exponential (turbulent solution, blue line) components, and a solution of Alexeev hydrodynamics equations,

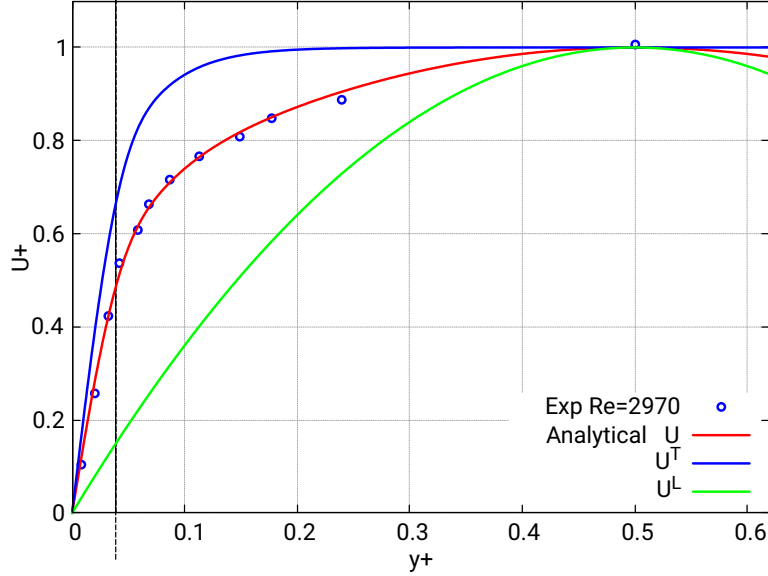


Figure 2: Comparison with Wei (1989) experiments at $Re = 2970$: the mean streamwise velocity (circles), the Navier-Stokes laminar solution U^L for the streamwise velocity (parabolic function, green line), the turbulent U^T solution the streamwise velocity (super-exponential function, blue line), and their superposition U , the solution of the Alexeev hydrodynamic equations. The solution U fits the experimental data well. The vertical black line shows the value of δ .

U (red line), that is a linear superposition of U^L and U^T for $\gamma = 0.65$ and $\delta = 0.04$. The solution of Alexeev hydrodynamics equations provides better fit to experimental data, than the Navier-Stokes solution.

The vertical black line shows the value of δ , that presents the boundary layer thickness scale, where the linear velocity profile ends. It was found [22, 23] that δ coincides with the Kolmogorov microscale, observed in experiment by Koseff and Street (1984) for 3D lid driven cavity flow [25].

We also plot the velocities in (U^+, y^+) coordinates, as presented in Wei (1989) paper. The parameter $y^+ = yU_\tau/\nu$, where U_τ is so called friction velocity, y is the absolute distance from the wall, and ν is the kinematic viscosity. One can interpret y^+ as a local Reynolds number. The friction velocity U_τ is defined as

$$u_\tau = \sqrt{\tau_w/\rho}, \quad (40)$$

where wall shear stress τ_w , $\tau_w = \rho\nu\frac{dU}{dy}$ at $y=0$, and the dimensionless velocity is given by $U^+ = u/U_\tau$. The Figure 3 demonstrates that the superposition U provides an excellent fit to the experimental mean velocity profile in (U^+, y^+) as well. The vertical dashed black line shows the value of δ . Similar results for $Re=22776$ are presented in Figure 4, where the Navier-Stokes solution is far from the experimental data, and the solution of the Alexeev hydrodynamic equations is much closer to the data. Such (U^+, y^+) plots often provide the comparison with the classical logarithmic von Karman law,

$$U^+ = \frac{1}{k} \log(y^+) + B, \quad (41)$$

with $k = 0.41$, $B = 5.2$ (sometimes with slight variations).

The comparison with Wei (1989) experiments at other Reynolds numbers, and with another channel experiment by Pasch (2023) [28] are provided in [11].

5.2 Comparison of solutions for pipe flow

5.2.1 Van Doorne and Westerweel pipe experiment.

In van Doorne and Westerweel (2007) experiment, a circular pipe with an inner diameter of 40 mm and a total length of 28 m was used, so the ratio of diameter to length was $D/Length = 700$ [7]. The working fluid was tap water. Due to a well designed contraction and thermal isolation of the pipe, the flow can be kept laminar up to $Re = 60,000$. It was found that the Coriolis force affects the velocity profile, as leads to an asymmetry for $Re \geq 3,000$, as explained by Draad (1998) [8], so the orientation of

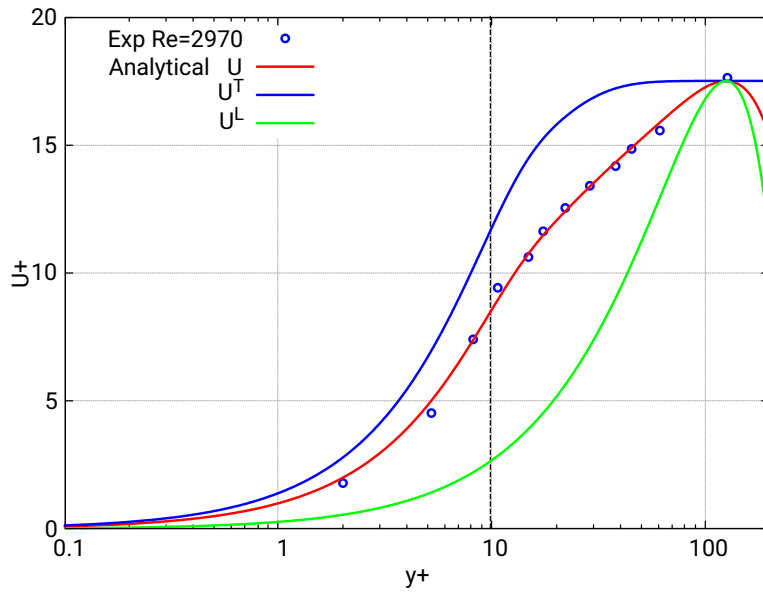


Figure 3: Comparison of streamwise mean velocity from Wei (1989) experiments in (Y^+, U^+) coordinates at $Re = 2970$ (circles) with the Navier-Stokes laminar solution U^L (parabolic solution, green line), THE turbulent solution U^T (super-exponential solution, blue line), and their superposition U (solution of the Alexeev hydrodynamic equations). The vertical dashed black line indicates δ .

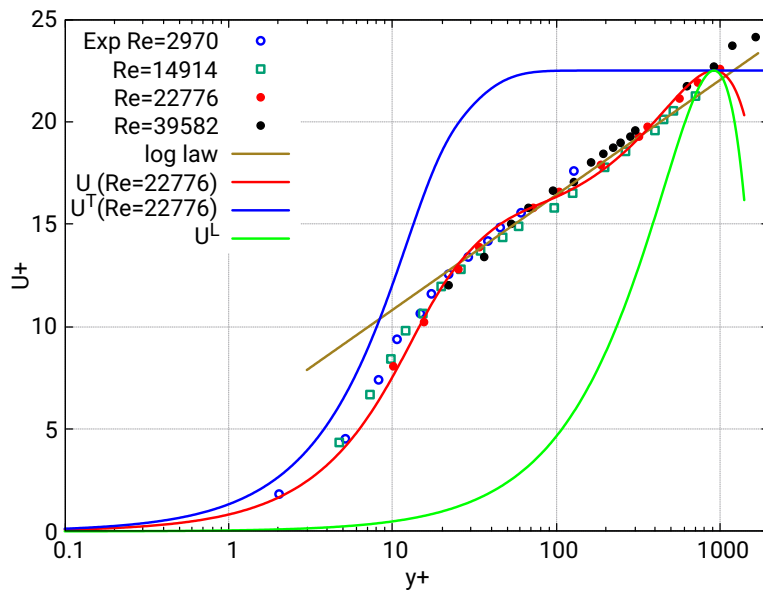


Figure 4: Velocity profiles for turbulent flow in channel: the experimental data (dots) by Wei (1989) [32], analytical solution of the Navier-Stokes laminar solution (parabolic function, green line) U^L , turbulent U^T solution (super-exponential function, blue line), and Alexeev hydrodynamic equations solution U (red line), the superposition of U^L and U^T , for Reynolds number $Re=22776$, that fits well the experimental data (red dots) for $Re=22776$. The log law by von Karman, $U^+ = 1/k \log(y^+) + B$ (log law) is shown as olive-green line.

the experimental pipe was chosen to exclude the Coriolis force. The measurements at $Re=7200$ were carried out at the distance of 26 m from the inlet, and stereoscopic-PIV was used [7]. The analytical solution (39) can be applied to circular pipe flow, when $\delta = \sqrt{\tau_0 \nu} / L_0 \ll 1$, which is the case, as $\delta = 0.047$. Figure 5 shows the experimental data for the streamwise mean velocity digitized from [7] along with several plots: (i) Navier-Stokes solution, the laminar (parabolic) flow profile (green line), (ii) turbulent (superexponential) flow profile (blue line) and (iii) the AHE solution (red line). The value of γ is $\gamma = 0.68$, obtained from minimal viscous dissipation principle [12]. One can see that neither the laminar nor turbulent solution fit the data, but the superposition given by equation (39), the AHE solution (red line), provides good comparison to the experimental data.

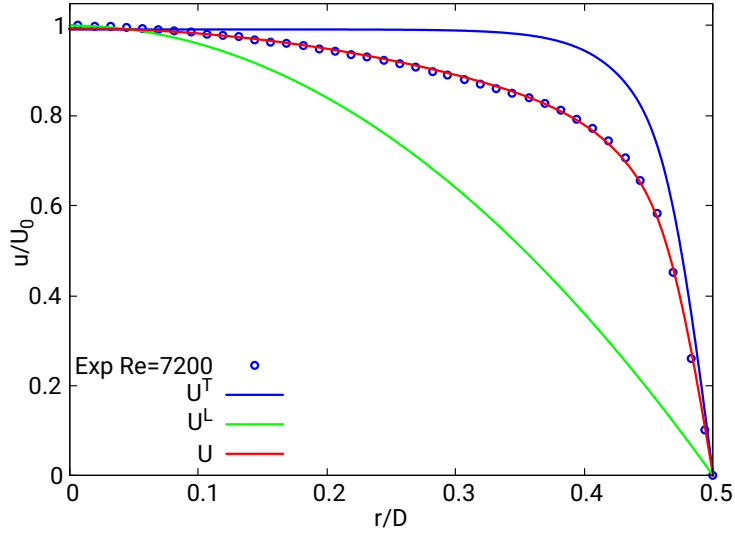


Figure 5: Comparison of experimental data for streamwise mean velocity $U_{exp} = u/U_0$ versus radius r/D (D is the diameter) (blue circles) for the van Doorne experiment [7] at $Re=7200$ with the laminar (parabolic) solution U^L of the Navier-Stokes equations (green line), the turbulent (super-exponential) solution U^T (blue line), and the solution U of the Alexeev hydrodynamic equations (red line). The analytical solution U fits the experimental velocity profile well, while other solutions deviate significantly from the data.

5.2.2 Superpipe experiments by Zagarola, Smits, Orszag and Yakhot. A series of 26 experiments was conducted using the Princeton Superpipe setup, with air as the working fluid [33]. The circular pipe diameter was 12.9 cm. The temperature was near ambient (295-300 K), and the pressure was varied between 1 and 186 atmospheres for 26 different experiments at Reynolds numbers, ranging from $3.15 \cdot 10^4$ to $35.2 \cdot 10^6$. The effects of the Coriolis force which potentially can affect the results, according to [7] and [8], were not discussed by the authors of [33].

The experimental conditions (pressure, density, viscosity, pressure gradient and timescale τ) varied by several orders of magnitude. However, the analytical solution parameters, γ and δ , did not vary significantly and remained within $0.6 < \gamma < 0.7$ and $0.003 < \delta < 0.006$.

Analytical solutions were constructed for all 26 experiments, and three representative examples are presented for comparison at the lowest, highest, and intermediate Reynolds numbers.

Figure 6 shows the streamwise velocity in turbulent Superpipe experiment for the minimum Reynolds number $Re = 3.15 \cdot 10^4$, the intermediate $Re = 1.02 \cdot 10^6$, and the maximum $Re = 35.2 \cdot 10^6$, along with the analytical solution U for each case. The laminar solution U^L (Navier-Stokes) and turbulent solution U^T are shown only for the experiment at $Re = 3.15 \cdot 10^4$.

The von Karman log law is also shown (olive - green line). The coefficients for the von Karman law (41) differ here: $k=0.44$ and $B=6.3$, as chosen by the authors of the experiments [33]. The von Karman law is limited to the region where the fluid mixes intensively, missing the near-wall and near-middle (buffer layer) region at $y^+ < 30$ and the outer region (nonlinear and essentially inviscid) that begins at $y^+ > 200$ (for $Re = 3.15 \cdot 10^4$). The log-law error in the buffer layer is 30%, and the error in the outer region is 6%.

The AHE analytical solution shows agreement with the experimental data within 3% as observed at the highest Reynolds number, while the other solutions (U^L and U^T) deviate significantly from the data.

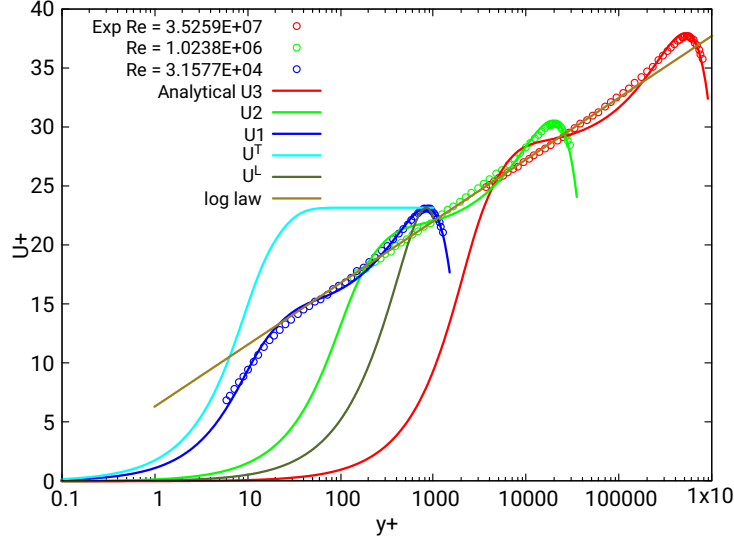


Figure 6: Comparison of the streamwise velocity in turbulent pipe flow from the Princeton Superpipe experiment [33], $Re = 3.15 \cdot 10^4$ (blue circles), $Re = 1.02 \cdot 10^6$ (green circles), and $Re = 3.52 \cdot 10^7$ (red circles). The analytical solution U is shown for each case in the corresponding color. The laminar solution U^L and turbulent solution U^T are shown for $Re = 3.15 \cdot 10^4$ only. The log law by von Karman, $U^+ = 1/k \log(y^+) + B$ (log law) is shown by olive-green line. The maximum error of 3% for AHE solution was observed at the highest Reynolds number.

6 Discussion

6.1 From Boltzmann to Navier-Stokes equations

The theoretical models for hydrodynamic flows fall under Hilbert's 6th problem [26], addressing the transition from the "atomistic view to the laws of motion of continua". It includes at least two steps:

(1) from mechanics to kinetics (from Newton to Boltzmann),
and

(2) from kinetics to mechanics and nonequilibrium thermodynamics of continua (from Boltzmann to Euler and Navier-Stokes), Gorban and Karlin (2014) [24].

It is considered that the first step, from mechanics to kinetics (from Newton to Boltzmann), was completed with the complexity approach to randomness invented by Solomonoff and Kolmogorov, as remarked in [24] (see the review [34] and the textbook [27]).

As for the second step, from kinetics to hydrodynamics and nonequilibrium thermodynamics of continua (from Boltzmann to Euler and Navier-Stokes), a review of mathematical works in this area shows that the well-known Euler and Navier-Stokes equations are valid only at "a limit of very slow flows with very small gradients of all fields, i.e., almost no flow at all", Gorban and Karlin (2014) [24].

This may explain why, in the turbulent flow experiments presented above, the NS solutions deviate significantly from the experimental data, as the flow velocities are not small.

6.2 Superposition coefficients γ

The superposition coefficients γ and $(1 - \gamma)$ were calculated using the principle of minimal viscous dissipation of kinetic energy ε_T relative to the shear stress (derivative of U) on the wall [12]. The minimum of ε_T gives a solution for γ :

$$\varepsilon_T = \frac{1}{U_y(0)^2} \int_0^L U_y^2 dy \cdot \frac{1}{L} \int_0^L U dy, \quad (42)$$

where $U(y)$ is presented by Eq.(39). The value of γ obtained by this procedure yields the best agreement between $U(y)$ and the experimental measurements. The parameter γ was within the interval from 0.6 to 0.7 for most of the cases considered, with both water and air as a working fluid.

6.3 Boundary layer thickness scale δ

The boundary layer thickness scale and the similarity parameter $\delta = \sqrt{\tau_0 \nu} / L_0$ is the most important parameter for the turbulent flows, discovered in the analytical solution. The value of δ coincides with the Kolmogorov microscale, observed in experiment by Koseff and Street (1984) for 3D lid driven cavity flow [25].

The parameter δ is a material property and does not depend on the Reynolds number, as shown by the data from the Wei and Willmarth experiment [32]: the experimental data for four different Reynolds numbers ranging from $Re=2910$ to $Re=39582$ collapse closely onto the same curve, as shown in Figure 4.

The value of δ is approximately 0.6 mm for distilled water and approximately the same for air over a wide pressure range. Knowing δ , one can determine the timescale parameter τ_0 , which is also a material property (though this parameter to be of lesser importance).

6.4 Turbulent boundary layer

The analytical solution U from equation (39) represents the turbulent boundary layer across all regions with great accuracy, as shown in Figure 4 (the analytical solution at $Re=22776$ is the red line; the Wei (1989) experiment is shown as red dots), with the linear law at the wall in the range $0 < y^+ < 5$, where U^L is negligible.

In the near-wall (buffer layer) region at $5 < y^+ < 30$, the solution U is strictly nonlinear, yet the analytical solution fits the flow data well. In the far-middle (inner) boundary layer region at $30 < y^+ < 200$, U^T is almost constant, while the solution (red line) exhibits variation due to the increasing contribution of the laminar component U^L . In this region, the AHE solution is a parabolic function that provides a closer fit to the experimental data (red dots) than the classical logarithmic von Karman law (olive-green line).

The outer region (nonlinear and essentially inviscid) begins at $y^+ > 200$ and extends to the centerline, where the analytical solution also shows good agreement with the experimental data.

6.5 Turbulence source and control

The turbulent component of the streamwise velocity U^T becomes zero, when the transverse velocity is zero in equation (26). In this case, the flow remains laminar and free of turbulence. The transverse velocity V^T is proportional to the transverse pressure gradient p_y^T in equation (33). Thus, the transverse pressure gradient and transverse velocity are the sources of turbulence. Experiments by van Doorne (2007) showed that the flow can be kept laminar up to $Re = 60,000$ by suppressing pressure disturbances at the inlet.

Turbulent flow can be converted to laminar flow by eliminating the transverse velocity component. This reveals a practical control mechanism: by applying controlled suction or injection through an array of small holes in the wall, the transverse velocity can be driven toward zero, thereby suppressing turbulence [10]. Suction removes fluid normal to the wall, while injection introduces fluid; both serve to manipulate the transverse flow component.

While the effectiveness of wall suction and injection for turbulence control has been observed experimentally, we provide the first rigorous theoretical explanation of the underlying mechanism, connecting transverse velocity suppression directly to the transition from turbulent to laminar flow. Remarkably, the suction or injection velocities required are approximately one thousand to ten thousand times smaller than the main streamwise velocities [10, 30].

7 Conclusion

The analytical solution of the Alexeev Hydrodynamic Equations for turbulent channel flow demonstrates significantly better agreement with the mean velocity experimental data than solutions obtained from the Navier-Stokes equations. These solutions successfully capture the correct velocity behavior across the entire turbulent boundary layer and into the external flow, spanning from the inner viscous sublayer to the outer layer of the boundary layer. The analytical solution reveals an important boundary layer thickness scale through the similarity parameter δ , which coincides with the Kolmogorov microscale observed in experiments. The mechanisms for turbulence generation were identified and a turbulence control method was proposed.

References

- [1] Alexeev B.V. The generalized Boltzmann equation, generalized hydrodynamic equations and their applications. Phil. Trans. Roy. Soc. London, 1994; A349, 417-443.
- [2] Alexeev B.V. Generalized Boltzmann Physical Kinetics, Elsevier, 2004.
- [3] Amosova E.V. Regularity of the Pressure Function for Weak Solutions of the Nonstationary Navier-Stokes Equations, Differential Equation, 2023; v59, 9, 1199 - 1215.
- [4] Ananiev P.A., Volkov P.K., Natural convection in vertical channel and cylinder by heating from below, Computational Mathematics and Mathematical Physics, 2004; v.16. 11.89-100 (in Russian).

- [5] Ananiev P.A., Volkov P.K., Coherent Structures and Jets in Natural-Convection Flows, High Temperature, 2006; Vol.44, No.3, 422-431.
- [6] Ananiev P.A., Volkov P.K., Investigation of natural convection flows with unstable temperature stratification, Computational Mathematics and Mathematical Physics, 2005; v.45. 7.1289-1303 (in Russian).
- [7] Van Doorne C.W.H., Westerweel J. Measurement of laminar, transitional and turbulent pipe flow using Stereoscopic-PIV, Experiments in Fluids, 2007, 42(2).
- [8] Draad A.A., Nieuwstadt F.T.M. The earth's rotation and laminar pipe flow. J. Fluid Mech., 1998, 361, 297-308.
- [9] Farrell P.E., Birkisson A., Funke S. W., Deflation Techniques for Finding Distinct Solutions of Nonlinear Partial Differential Equations. SIAM Journal on Scientific Computing, 2015; Vol.37, Iss.4 .
- [10] Fedoseyev A. Controlling Turbulent Boundary Layer Flow through the Transverse Velocity Component, Chapter in book: Boundary Layer Flows - Control Techniques and Technological Applications, ISBN 978-1-83634-298-4, Ed. Zambri Harum (in print), <https://www.intechopen.com/>
- [11] Fedoseyev A. Improved Analytical Solution for Turbulent Flow in Channel and Circular Pipe, J. Phys.: Conf. Ser. 2025, 3145 012011.
- [12] Fedoseyev A. Minimization Principle for Analytical Solution of Turbulent Flow in Channel, J. Phys.: Conf. Ser. 2024; 2910 012012.
- [13] Fedoseyev A. Analytical Solution for Transverse Velocity of Turbulent Flow in Channel, J. Phys.: Conf. Ser. 2024; 2910 012013.
- [14] Fedoseyev A. Approximate Analytical Solution for Turbulent Flow in Channel, J. Phys.: Conf. Ser. 2023, 2675 012011.
- [15] Fedoseyev A., Finite element method stabilization for supersonic flows with flux correction transport method, AIP CP 2302, 120003 (2020), Ed. M.Todorov.
- [16] Fedoseyev A., Griaznov V., Ouazzani J., Simulation of rarefied hypersonic gas flow and comparison with experimental data II, Proc. AMITANS-2022 Conf., AIP CP 2953, 2023; Ed. M.Todorov.
- [17] Fedoseyev A., Griaznov V., Simulation of Rarefied Hypersonic Gas Flow and Comparison with Experimental Data, AMiTANS-2021 Conf. Proc., AIP CP 2522, 2021; Ed. M.Todorov.
- [18] Fedoseyev A., Alexeev B.V. Generalized hydrodynamic equations for viscous flows-simulation versus experimental data, AMITANS-2012 Conf. Proc., AIP CP 1487, 2012, 241-247.
- [19] Fedoseyev A.I., Alexeev, B.V. Simulation of viscous flows with boundary layers within multiscale model using generalized hydrodynamics equations, Procedia Computer Science, 2010, 1, 665-672.
- [20] Fedoseyev A.I. A Regularization approach to solving the Navier-Stokes equations for problems with boundary layer, Japanese Comput. Fluid Dynamics. J. Spec. Issue, 2001 (Proc. 8th ISCFD 1999 at ZARM, Bremen), 317-324.
- [21] Fedoseyev A.I., Kansa E.J., C. Marin, and A.G. Ostrogorsky, Japanese Computational Fluid Dynamics Journal, 2001; 10(3), 325-333.
- [22] Fedoseyev A.I., Alexeev, B.V. Mathematical model for viscous incompressible fluid flow using Alexeev equations and comparison with experimental data. In: Dey, S.K., Ziebarth, G., Ferrandiz (Eds.), Proc. Advances in Scientific Computing Modelling (Special Proc. IMACS'98). Alicante, Spain, 1998; 158-163.
- [23] Fedoseyev A.I., Alexeev, B.V. Higher order continuum model for incompressible viscous flow and application to the modelling of thermal vibrational convection. In: Inan, E., Markov, K.Z. (Eds.), Continuum Models and Discrete Systems (CMD59) Proc. 9th Int. Symposium. Istanbul, Turkey, 1998; 130-137.
- [24] Gorban A.N., Karlin I., Hilbert's 6th problem: exact and approximate hydrodynamic manifolds for kinetic equations, American Mathematical Society, 2014; 51, 2, 187-246.
- [25] Koseff R., R. L. Street, The Lid-Driven Cavity Flow: A Synthesis of Qualitative and Quantitative Observations, Trans. ASME J. Fluids Engineering, 1984; 106, 390-398.

-
- [26] Hilbert, D. Mathematical problems, *Bull. Amer. Math. Soc.* 8, 1902; 10, 437-479.
- [27] Li M., Vitanyi P., *An introduction to Kolmogorov complexity and its applications*, 2nd ed., *Graduate Texts in Computer Science*, Springer-Verlag, New York, 1997.
- [28] Pasch S., Leister R., Gatti D. et al. Measurements in a Turbulent Channel Flow by Means of an LDV Profile Sensor, *Flow, Turbulence and Combustion*, 2024, 113, 195-213.
- [29] Powell M. J. D. An efficient method for finding the minimum of a function of several variables without calculating derivatives. *Computer Journal*. 1964; 7 (2): 155-162.
- [30] Schlichting, H., *Boundary Layer Theory*, Fourth edition, McGraw-Hill, New York, 1960.
- [31] Volkov P.K., About the nature of fluid motion, *Vestnik Yugorskogo Universiteta*, 2011; 2,1, 21p. (in Russian). <https://cyberleninka.ru/article/n/o-prirode-dvizheniya-zhidkostey/pdf> (last accessed July 13, 2025)
- [32] Wei T., Willmarth W.W. Reynolds-number effects on the structure of a turbulent channel flow, *J. Fluid Mech.*, 1989, vol 204, 57-95.
- [33] Zagarola M. V., Smits A.J., Orszag S.A., Yakhot V. Experiments in high Reynolds number turbulent pipe flow, *AIAA Paper 96-0654*, January 1996.
- [34] Zvonkin A. K., Levin L. A., The complexity of finite objects and the basing of the concepts of information and randomness on the theory of algorithms, *Uspehi Mat. Nauk* 25 (1970), no. 6 (156), 85-127.